# Downloaded from https://www.science.org at Rice University on August 16, 2022

### **QUANTUM GASES**

# Spin-charge separation in a one-dimensional Fermi gas with tunable interactions

Ruwan Senaratne<sup>1</sup>†, Danyel Cavazos-Cavazos<sup>1</sup>†, Sheng Wang<sup>2,3</sup>, Feng He<sup>3,4</sup>, Ya-Ting Chang<sup>1</sup>, Aashish Kafle<sup>1</sup>. Han Pu<sup>1</sup>. Xi-Wen Guan<sup>2,5</sup>\*. Randall G. Hulet<sup>1</sup>\*

Ultracold atoms confined to periodic potentials have proven to be a powerful tool for quantum simulation of complex many-body systems. We confine fermions to one dimension to realize the Tomonaga-Luttinger liquid model, which describes the highly collective nature of their low-energy excitations. We use Bragg spectroscopy to directly excite either the spin or charge waves for various strengths of repulsive interaction. We observe that the velocity of the spin and charge excitations shift in opposite directions with increasing interaction, a hallmark of spin-charge separation. The excitation spectra are in quantitative agreement with the exact solution of the Yang-Gaudin model and the Tomonaga-Luttinger liquid theory. Furthermore, we identify effects of nonlinear corrections to this theory that arise from band curvature and back-scattering.

nlike three-dimensional (3D) metals whose low-energy excitations are fermionic quasiparticles, the low-energy excitations of 1D fermions are collective bosonic spin- and charge-density waves (SDWs and CDWs) that disperse linearly, as described by the Tomonaga-Luttinger liquid (TLL) theory (1–5). Notably, the SDWs and the CDWs of an interacting 1D Fermi gas propagate at different speeds, causing a spatial separation of the spin and charge excitations in the gas.

Spin-charge separation has been studied in quasi-1D solid-state materials in several ground-breaking experiments that used either momentum-resolved tunneling to determine the dispersions (6-8) or angle-resolved photoemission spectroscopy (9-11). Although these experiments observe splitting into spin and charge excitations, a quantitative analysis of these data has proved challenging because of the complexity of the electronic structure and the unavoidable presence of impurities and defects. Recently, a series of experiments with ultracold atoms in an optical lattice was performed on a single-site resolved 1D Hubbard chain, leading to the observation of the fractionalization of spin and charge quantum numbers at equilibrium (12), the modification of the SDW wave vector by density doping and by spin polarization (13), and the study of simultaneous spin and charge dynamics outside the Luttinger liquid regime that result from a deconfinement-induced quench (14). These experiments demonstrated the ability to perform quantum simulation of interacting fermions in one dimension with unprecedented control in cold-atom systems, but they did not measure the collective low-energy excitation spectrum inherent to spin-charge separation.

The excitation spectrum of the charge (density) mode of fermionic atoms confined to quasi-1D tubes has been previously measured for fixed (15) and variable interaction strengths (16). These experiments used two-photon stimulated Bragg spectroscopy (Fig. 1, A and B) to impart an observable momentum  $\hbar q$ , with energy  $\hbar\omega$ , while keeping the internal state of the atom unchanged (17-20) (ħ is the reduced Planck's constant). The response of the 1D gas at a particular q and  $\omega$  is related to the dynamic structure factor (DSF)  $S(q, \omega)$ , which characterizes the low-energy excitation spectrum for  $q \ll k_{\rm F}$ , where  $k_{\rm F}$  is the Fermi wave vector. In our previous work the charge-mode structure factor  $S_c(q, \omega)$  was measured and quantitatively compared with theory with good results (16). Measurement of the spin-wave spectrum  $S_s(q, \omega)$  remained out of reach because, without appropriate modifications, such a measurement induces single-photon scattering events that produce substantial atom loss.

We have developed improvements to our implementation of Bragg spectroscopy to reduce spontaneous scattering to an acceptable

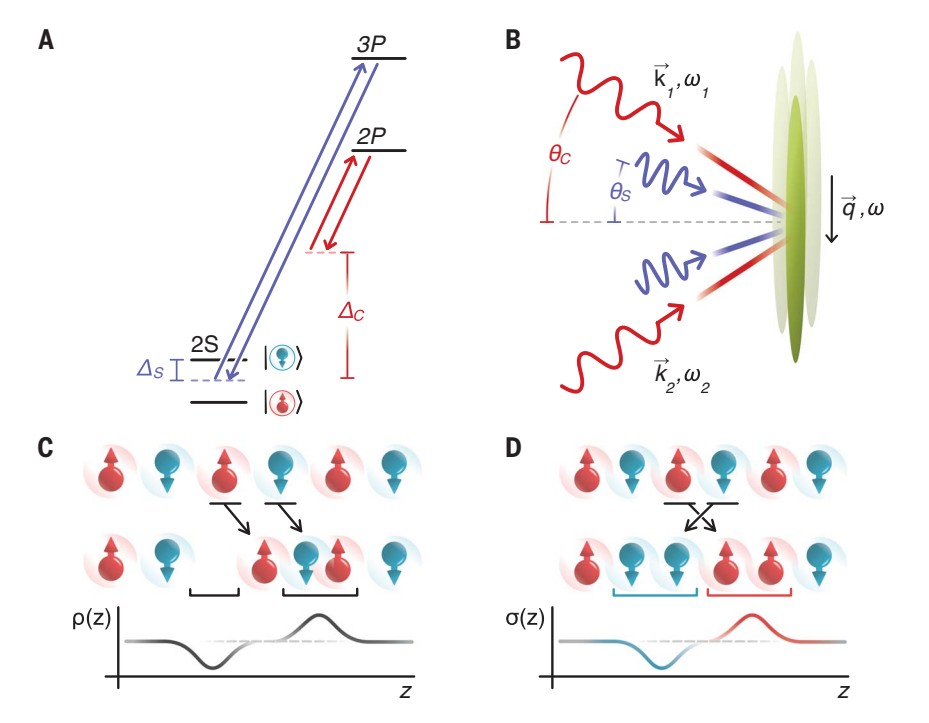


**Fig. 1. Spin and charge excitations from Bragg spectroscopy.** (**A**) Partial energy-level diagram of  $^6$ Li showing relevant transitions and laser detunings for spin ( $\Delta_s$ , violet) and charge ( $\Delta_c$ , red) excitations. (**B**) Relative orientation ( $\theta_{c,s}$ ) of each Bragg beam (1 and 2) with respect to the axis perpendicular to the 1D tube direction. A momentum transfer  $\vec{q} = \vec{k}_1 - \vec{k}_2 \approx 0.2~k_F$  for the central tubes is delivered to the sample for a given relative detuning  $\omega = \omega_1 - \omega_2$  between the beams. (**C** and **D**) Diagram of the charge and spin excitations, showing an excitation of (C) a particle-hole pair and (D) a spinon pair. The effect on the total density  $\rho(z)$  and spin density  $\sigma(z)$  is shown for each case at the bottom. The excitations are depicted, for clarity, as starting from a classical zero-temperature antiferromagnetic ground state in the strongly repulsive regime.

<sup>1</sup>Department of Physics and Astronomy, Rice University, Houston, TX 77005, USA. <sup>2</sup>State Key Laboratory of Magnetic Resonance and Atomic and Molecular Physics, Wuhan Institute of Physics and Mathematics, APM, Chinese Academy of Sciences, Wuhan 430071, China. <sup>3</sup>University of Chinese Academy of Sciences, Beijing 100049, China. <sup>4</sup>International School for Advanced Studies (SISSA) and National Institute of Nuclear Physics (INFN), Sezione di Trieste, 34136 Trieste, Italy. <sup>5</sup>Department of Theoretical Physics, RSPE, Australian National University, Canberra, ACT 0200, Australia.

\*Corresponding author. Email: randy@rice.edu (R.G.H.); xiwen.guan@anu.edu.au (X.-W.G.)

†These authors contributed equally to this work

level while selectively exciting either the SDW or the CDW with tunable repulsive interactions. The measurements are compared with the TLL theory, which describes the lowenergy excitations of the more general Yang-Gaudin model of a spin-1/2, 1D Fermi gas with repulsive delta-function interactions in the continuum limit (21, 22). They provide a quantitative test of spin-charge separation in the Luttinger liquid regime. Additionally, we quantitatively show that our results for  $S_{\rm s}(q,\,\omega)$  provide evidence for deviations from the linear TLL theory caused by low-energy back-scattering interactions, which are usually neglected to obtain a linear spin-mode dispersion (5).

Bragg spectroscopy is well suited to studying spin-charge separation because the CDW or SDW may be isolated by the choice of detuning of the Bragg beams from resonance with an electronic excited state (Fig. 1). The detuning determines the sign of the light-shift potential, which can be used to create a symmetrical light shift that exclusively excites charge waves or an asymmetrical potential that only excites spin waves. For a system composed of a balanced mixture of two spin components ( $\uparrow$ ,  $\downarrow$ ) we can identify two independent contributions to the DSF,  $S_{\uparrow\uparrow}$  and  $S_{\uparrow\downarrow}$ , and thus define a charge- and spin-density DSF given by (5)

$$S_{\mathrm{c,s}}(q,\omega) \equiv 2 \big[ S_{\uparrow\uparrow}(q,\omega) \pm S_{\uparrow\downarrow}(q,\omega) \big]$$

where the "+" sign corresponds to charge and the "-" sign corresponds to spin. At zero temperature, the momentum transfer to the system from the Bragg beams is given by (20, 23)

$$P(q,\omega)$$
  $\propto \left(rac{1}{\Delta_{\uparrow}^2} + rac{1}{\Delta_{\downarrow}^2}
ight)\!S_{\uparrow\uparrow} + rac{2}{\Delta_{\uparrow}\Delta_{\downarrow}}S_{\uparrow\downarrow}$ 

where  $\Delta_{\sigma}$  is the relative detuning of the Bragg beam from the excited state with respect to each ground spin state  $\sigma$ . If the condition  $\Delta_{\uparrow} \approx \Delta_{\downarrow} \gg \Delta_{\uparrow\downarrow}$  is satisfied, where  $\Delta_{\uparrow\downarrow}$  is the splitting of the spin states, then  $P(q, \omega) \propto$  $S_c(q, \omega)$  and a CDW is excited, as depicted in Fig. 1C. On the other hand, if  $\Delta_{\uparrow} = -\Delta_{\downarrow} =$  $|\Delta_{\uparrow\downarrow}|/2$ , then  $P(q,\omega) \propto S_{\rm s}(q,\omega)$  and an SDW is excited, as depicted in Fig. 1D. The detuning required for measuring  $S_s(q, \omega)$  is thus fixed by  $\Delta_{\uparrow\downarrow}$ , unlike in the case for measuring  $S_{\rm c}(q,\omega)$ , where, in principle, the detuning may be arbitrarily large. In the finite temperature case, a reverse Bragg process must also be considered, for which the momentum transfer is modified as  $P(q, \omega) \propto S(q, \omega) - S(-q, -\omega) =$  $S(q, \omega)[1 - \exp(-\hbar\omega/k_BT)]$  (24, 25), where  $k_B$ is the Boltzmann constant.

To reduce spontaneous scattering during the Bragg measurement, the ratio of  $\Delta_{\uparrow\downarrow}$  to  $\Gamma$ , the linewidth of the transition, must be increased. We approximately doubled  $\Delta_{\uparrow\downarrow}$  by

choosing  $|1\rangle$  and  $|3\rangle$  as our pseudo-spin-1/2 states, rather than  $|1\rangle$  and  $|2\rangle$  as used previously (states  $|1\rangle$ ,  $|2\rangle$ , and  $|3\rangle$  are the three lowest hyperfine states of <sup>6</sup>Li) (16, 19). For the excitation of the SDW, we took the additional step of reducing  $\Gamma$  by detuning the Bragg beams from the  $3P_{3/2}$  excited state at a wavelength of 323 nm, rather than the usual 671-nm transition to the  $2P_{3/2}$  state that we use to excite the CDW (see Fig. 1A). The spontaneous-decay linewidth of the ultraviolet transition is nearly eight times smaller than that for the red transition (26). We compensate for the difference in wavelength by simply adjusting the angle between the Bragg beams ( $\theta_c \simeq 4.5^{\circ}$  and  $\theta_s \simeq 2.2^{\circ}$ ; see Fig. 1B), such that for both cases, the Bragg wave vector is parallel to the tube axis and has a magnitude  $|\vec{q}| = 1.47 \, \mu \text{m}^{-1}$ , corresponding to  $0.2k_{\rm F}$  for a peak-occupancy tube. Thus, the net effect of this change is to further reduce the rate of incoherent scattering. The combination of these two steps reduces the spontaneous scattering by more than a 10-fold factor for a given Bragg coupling, as compared with (16), and is sufficient to measure  $S_s(q, \omega)$ .

A more detailed description of our experimental methods may be found in the supplementary materials (27). We prepare a spin-balanced mixture of <sup>6</sup>Li atoms in the two energetically lowest hyperfine sublevels, states  $|1\rangle$  and  $|2\rangle$ , and confine them in an isotropic optical trap. We evaporatively cool the atoms to a temperature  $T \approx 0.1T_F$ , where  $T_F$  is the Fermi temperature. We create an effectively 1D system that realizes the Yang-Gaudin model by loading the atoms into a 2D optical lattice with depth of  $15E_r$ , where  $E_r$  is the recoil energy of a lattice photon of wavelength 1.064 um. The resulting trap configuration is an array of quasi-1D tubes that are elongated in the axial dimension with an aspect ratio of ~170.

The number of atoms per tube is nonuniform across the ensemble of tubes because of the Gaussian curvature of the optical beams.

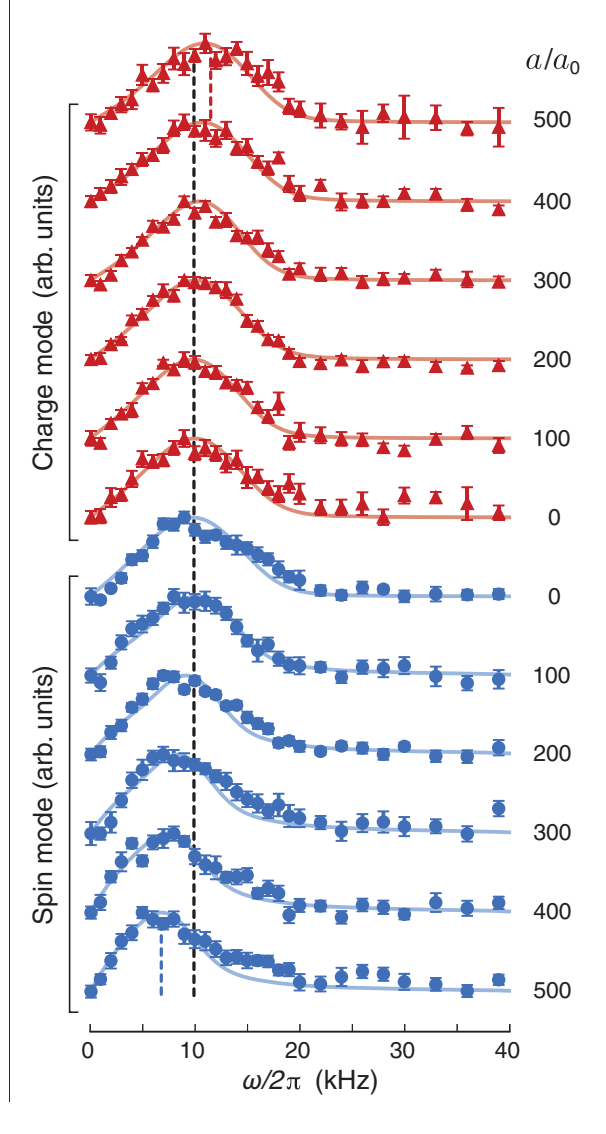
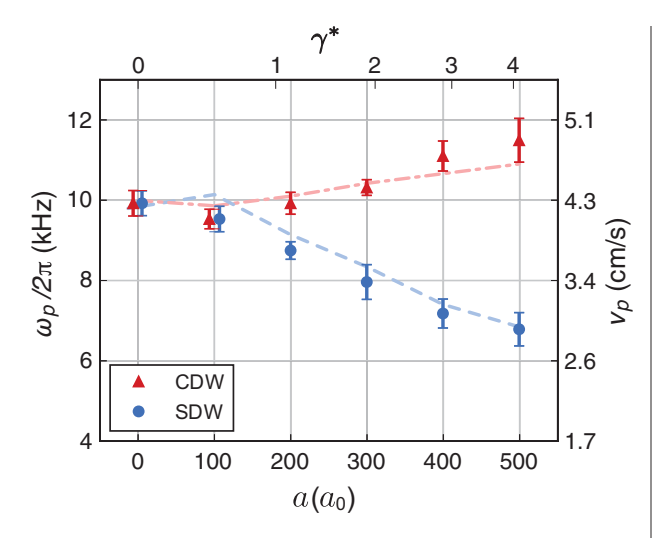


Fig. 2. Bragg spectra. Normalized Bragg signals related to  $S_c(q, \omega)$  (red triangles) and  $S_s(q, \omega)$  (blue circles) for the range of 3D scattering length a from 0 to  $500a_0$ . Each data point is the average of at least 20 separate experimental shots. Error bars represent standard error, obtained by bootstrapping (40). Vertical dashed lines show the extracted peak frequency  $\omega_p$  for the noninteracting case (black) and the strongest probed interactions for the spin and charge modes (blue and red. respectively). Solid lines are the calculated Bragg spectra for a global temperature T = 250 nK with no additional fitting parameters other than overall scaling. Theory includes the nonlinear effects of band curvature in the charge mode and back-scattering in the spin mode (for linear theory, see figs. S7 and S8). Deviations from theory at high frequency may be due to unaccounted-for corrections of

### Fig. 3. Spin-charge separation.

Peaks of measured Bragg spectra for charge (red triangles) and spin (blue circles) configurations for a ranging from 0 to  $500a_0$ . Peak frequency values were determined through fits of a parabolic function to the data points above 50% of the maximum measured value, and error bars are statistical standard errors of the relevant fit parameters. The corresponding speed of sound  $v_p = \omega_p/q$  is given by the right axis. The upper horizontal axis gives the interaction strength in terms of the Lieb-



Liniger parameter  $\gamma^*$ , evaluated at the center of a tube with an occupancy of 30 atoms. Lines show the calculated values for  $\omega_p$  for the charge and spin modes (dash-dotted red and dashed blue lines, respectively). Symbols for  $\alpha=0$  and  $100\alpha_0$  have been slightly displaced horizontally from one another for clarity. Nonmonotonicity in the charge-mode data and theory at low interaction is caused by small residual differences in the number profiles prepared at different interaction strengths. Nonmonotonicity in the spin-mode theory is likely a consequence of neglecting the effects of band curvature, a  $q^3$  correction.

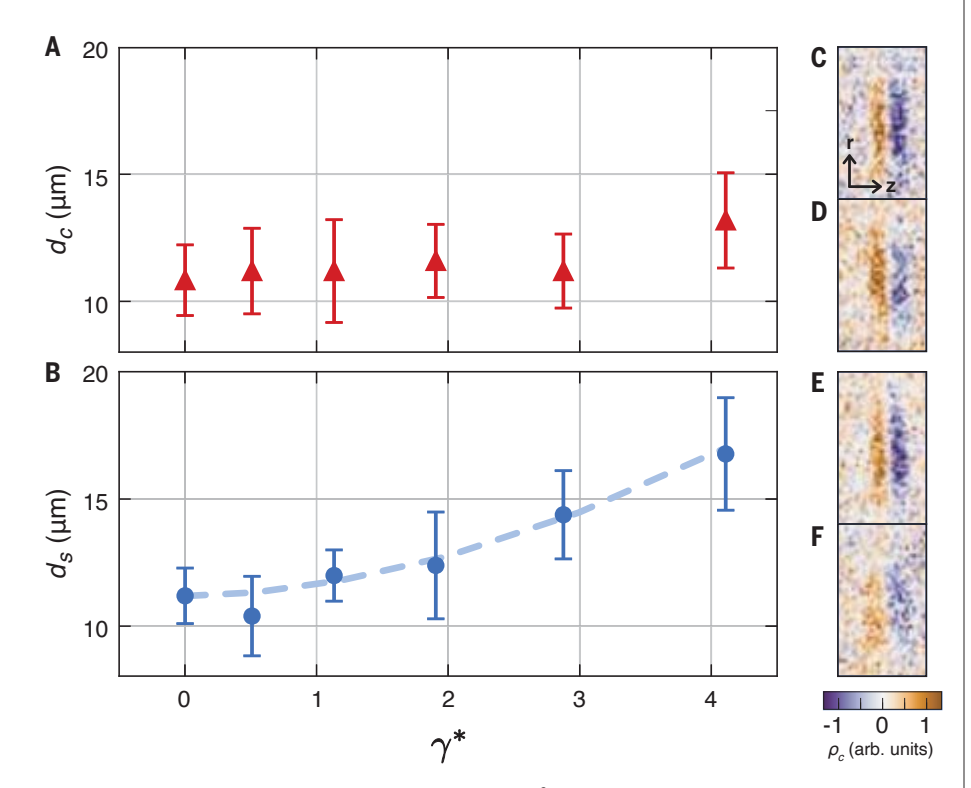


**Fig. 4. Dispersion of SDWs and CDWs.** (**A** and **B**) The  $1/e^2$  axial width of outcoupled atoms after a Bragg pulse and 150-μs time of flight for (A) charge ( $d_c$ , red triangles) and (B) spin ( $d_s$ , blue circles) excitations, with a ranging from 0 to  $500a_0$ . The widths are the Gaussian fits to the positive outcoupled signal at  $ω_p$ . Error bars are standard errors determined by bootstrapping for at least 20 independent images (40). The horizontal axis gives the Lieb-Liniger parameter  $γ^*$  calculated for a median tube occupancy of 30 atoms (27). The blue dashed line shows an estimation for  $d_s$  derived from the finite lifetime of the spin bosons. (**C** to **F**) Representative samples of column-density ( $ρ_c$ ) images of the atom cloud after the Bragg pulse and time of flight. Shown are the charge-mode excitations with (C) a = 0 and (D)  $a = 500a_0$ , and the spin-mode excitations with (E) a = 0 and (F)  $a = 500a_0$ . Each frame corresponds to 40 μm by 65 μm.

The number distribution from tube to tube is also dependent on interaction strength; the central tube occupancy is highest for a noninteracting gas and decreases as repulsive interactions increase. We actively control for these variations by applying a focused repulsive green (532 nm) laser beam during the lattice ramp up along each of the three orthogonal axes (28). Varying the depth of this harmonic antitrapping potential allows us to adjust the amount of confinement produced by the optical lattice and thus make the density profiles comparable between different interaction strengths while keeping the total atom number constant. We measure the tube occupancy by taking in situ phase-contrast images of the atom cloud (29) and performing an inverse Abel transform to obtain the 3D distribution. A typical ensemble consists of a total of  $6.5 \times 10^4$  atoms, has a peak tube occupancy of ~50 atoms, and has a most probable tube occupancy of ~30 atoms.

We perform Bragg spectroscopy by applying the pair of Bragg beams on the atoms in a 200-us pulse. The intensity per beam is fixed to limit the loss of atoms caused by spontaneous scattering to 6 to 8% during the spin-mode measurement and to ensure that the momentum transfer is in the linear-response regime for either mode over the entire range of interaction strengths that we study (27). There is no discernible atom loss during the chargemode measurement. Immediately after the Bragg pulse, the atoms are released from the lattice and are imaged using phase-contrast imaging after 150 us of time of flight, after which atoms receiving the Bragg kick are noticeably displaced from the center of the cloud (fig. S1). We define the Bragg signal to be proportional to the number of outcoupled atoms.

The interaction strength is readily tunable using the Feshbach resonance between states  $|1\rangle$  and  $|3\rangle$  located at 690 G (30). The 3D scattering length a may be tuned between a = 0and  $a = 500a_0$ , where  $a_0$  is the Bohr radius, without appreciable atom loss. Figure 2 shows the measured (symbols) and calculated (solid lines) Bragg spectra for both modes in the range of a from 0 to  $500a_0$ . Our DSF calculations take into account the effect of the inhomogeneous density that stems from the harmonic confinement along each tube by use of the local density approximation (LDA). The strength of interactions is density dependent and is given by the dimensionless Lieb-Liniger parameter  $\gamma = mg_1(a)/\hbar^2 \rho_{1D}$ , where  $g_1(a)$  is the coupling strength of the quasi-1D pseudopotential (31) and m is the atomic mass. The local density  $\rho_{1D}$  determines the local Fermi velocity and momentum ( $v_{\rm F}$  and  $\hbar k_{\rm F}$ ), the Luttinger parameters  $(K_{c,s})$ , and the local velocities of the charge and spin waves ( $v_c$ and  $v_s$ , respectively). Because the Bragg signal

is proportional to the total transferred momentum, we sum up the local values of the DSF along each tube, by invoking the LDA, to obtain the calculated spectra. Finally, we account for the frequency broadening caused by the finite duration of the Bragg pulses. A global temperature of 250 nK is the only free parameter in this model, other than an independent normalization of each calculated and measured spectrum.

To calculate the charge and spin DSFs, we use the exact Bethe ansatz solution of the Yang-Gaudin model at zero temperature (21, 32). For  $|q| \ll k_{\rm F}$ , the low-energy charge and spin excitations have approximately linear dispersion and, in this approximation,  $S_{c.s}(q,\omega)$  \infty  $|q| \delta(\omega - v_{\rm c.s}q)$ . However, at finite temperature and q, these DSFs are broadened when nonlinear effects are considered (33). For the strength of interactions probed in this experiment and for  $T \ll T_F$ ,  $S_c(q, \omega)$  is well approximated by the noninteracting DSF because the latter also exhibits a particle-hole excitation spectrum with width  $\propto q^2$ . As in (16), the effect of interactions is accounted for by replacing  $k_{\rm F}$  with  $k_{\rm c}$  =  $m^*v_{\rm c}/\hbar$ , where  $m^*$  is the effective mass. The leading correction to the spin-mode dispersion at finite temperature is a consequence of a low-energy back-scattering process that is expected for contact interactions in 1D (34). Here, distinguishable spins permute between the two Fermi points by exchanging  $2k_{\rm F}$ . This process is exclusive to the spin sector and disrupts the linearization of the spin dispersion in the bosonization approach of TLL theory (5, 32). We obtain the retarded spin-spin correlation function at finite temperature from the dressed spinboson propagator (35). By comparing our measurements to the nonlinear Luttinger liquid (NLL) theory, we find that accounting for nonlinearities caused by back-scattering is necessary to model the spin Bragg spectra, particularly for large interactions. The linear TLL model fails to reproduce the observed high-frequency tails of the spin-mode Bragg spectra (27).

The frequency at which the Bragg signal reaches a maximum,  $\omega_{\!\scriptscriptstyle p}\!,$  corresponds to the most probable value of the mode velocity,  $v_{\rm p}$  =  $\omega_{\rm p}/q$ , in the ensemble. We determine the peaks of each of the measured spectra by fitting a parabola to the data points that are above 50% of the maximum measured value for each spectrum. The locations of the peaks of the spectra obtained for our range of interaction are shown in Fig. 3 along with the peaks of the calculated spectra for each mode, which are in excellent agreement. For the noninteracting gas, the spin and charge collective modes have the same speed, resulting in nearly identical measured spectra for the two cases (27). The congruence between the two spectra also confirms that the atom loss suffered during the spin-mode measurement has no discernible effect on the measured Bragg spectrum. As the strength of the interaction is increased, the charge-mode velocity  $v_{\rm c}$  increases, whereas the spin-mode velocity  $v_{\rm s}$  decreases. This is seen in the shifts of the peaks of the two spectra: to a lower frequency for the spin mode, and to a higher frequency for the charge mode.

We further explored the NLL regime by extracting the axial width of the out-coupled atom packet after time-of-flight expansion, as shown in Fig. 4 as functions of interaction for both modes. As expected, the out-coupled widths increase with  $\gamma$  for measurements of the spin mode, whereas they remain approximately constant for the charge mode. We are able to model the increase in the out-coupled width for the spin mode by calculating the spread in velocities implied by the finite spin-boson lifetime due to back-scattering (27).

Having harnessed the tunability of interactions available in the cold-atom setting, we reveal the role of interactions in spin-charge separation by tuning between a spin-charge separated regime and one where there is no separation. Further, the selectivity of the Bragg process in exciting either the CDW or the SDW allows us to provide a clear demonstration of the division of the TLL Hamiltonian into distinct spin and charge sectors. Bragg spectroscopy may be used to probe the ultracold-atom TLL beyond the demonstration of spin-charge separation contained in this work. Measurements with variable q can be conducted to further study the NLL and to benchmark calculations that include effects of band curvature and spin-charge coupling (33, 35, 36). Additionally, at increased temperatures and interactions, a spin-incoherent Luttinger liquid is expected, which supports a propagating charge mode but not a spin mode (37, 38). Spin-imbalanced mixtures and attractive interactions are also of interest and are accessible by using this technique (39). Experiments with shallower lattices will allow for the study of dimensionality effects due to tunneling between tubes (5). It is increasingly clear that the oft-admired mathematical elegance of 1D manybody physics is well complemented by the purity and tunability of ultracold atoms.

### REFERENCES AND NOTES

- 1. S.-I. Tomonaga, *Prog. Theor. Phys.* **5**, 544–569 (1950).
- 2. J. Luttinger, J. Math. Phys. 4, 1154-1162 (1963).
- F. D. M. Haldane, *J. Phys. C Solid State Phys.* **14**, 2585–2609 (1981).
- 4. J. Voit, J. Phys. Condens. Matter 5, 8305-8336 (1993).
- T. Giamarchi, Quantum Physics in One Dimension (Oxford Univ. Press, 2003).
- 6. O. M. Auslaender et al., Science 295, 825-828 (2002).
- 7. O. M. Auslaender et al., Science 308, 88-92 (2005).
- 8. Y. Jompol et al., Science 325, 597-601 (2009).
- P. Segovia, D. Purdie, M. Hengsberger, Y. Baer, *Nature* 402, 504–507 (1999).
- 10. C. Kim et al., Phys. Rev. Lett. 77, 4054-4057 (1996).
- 11. B. Kim et al., Nat. Phys. 2, 397-401 (2006).

- 12. T. A. Hilker et al., Science 357, 484-487 (2017).
- 13. G. Salomon et al., Nature 565, 56-60 (2019).
- 14. J. Vijavan et al., Science 367, 186-189 (2020).
- 15. G. Pagano et al., Nat. Phys. 10, 198-201 (2014).
- 16. T. L. Yang et al., Phys. Rev. Lett. 121, 103001 (2018).
- 17. J. Stenger et al., Phys. Rev. Lett. **82**, 4569–4573 (1999).
- J. Steinhauer, R. Ozeri, N. Katz, N. Davidson, *Phys. Rev. Lett.* 88, 120407 (2002).
- G. Veeravalli, E. Kuhnle, P. Dyke, C. J. Vale, *Phys. Rev. Lett.* 101, 250403 (2008).
- S. Hoinka, M. Lingham, M. Delehaye, C. J. Vale, *Phys. Rev. Lett.* 109, 050403 (2012).
- 21. C. N. Yang, Phys. Rev. Lett. 19, 1312-1315 (1967).
- 22. M. Gaudin, Phys. Lett. A 24, 55-56 (1967).
- 23. D. Pines, Theory of Quantum Liquids: Normal Fermi Liquids (CRC Press, 2018).
- A. Brunello, F. Dalfovo, L. Pitaevskii, S. Stringari, F. Zambelli, Phys. Rev. A 64, 063614 (2001).
- A. Y. Cherny, J. Brand, *Phys. Rev. A* 73, 023612 (2006).
- 26. P. M. Duarte et al., Phys. Rev. A 84, 061406 (2011).
- 27. See supplementary materials.
- 28. R. A. Hart et al., Nature 519, 211-214 (2015).
- R. G. Hulet, J. H. V. Nguyen, R. Senaratne, Rev. Sci. Instrum. 91, 011101 (2020).
- 30. G. Zürn et al., Phys. Rev. Lett. 110, 135301 (2013).
- 31. M. Olshanii, *Phys. Rev. Lett.* **81**, 938–941 (1998).
- 32. F. He et al., Phys. Rev. Lett. 125, 190401 (2020).
- A. Imambekov, T. L. Schmidt, L. I. Glazman, Rev. Mod. Phys. 84, 1253–1306 (2012).
- F. D. M. Haldane, J. Phys. C Solid State Phys. 12, 4791–4799 (1979).
- R. G. Pereira, E. Sela, *Phys. Rev. B* 82, 115324 (2010).
   A. Imambekov, L. I. Glazman, *Science* 323, 228–231 (2009).
- 37. G. A. Fiete, Rev. Mod. Phys. 79, 801–820 (2007).
- P. Kakashvili, S. Bhongale, H. Pu, C. Bolech, *Phys. Rev. A* 78, 041602 (2008).
- X.-W. Guan, M. T. Batchelor, C. Lee, Rev. Mod. Phys. 85, 1633–1691 (2013).
- 40. B. Efron. Ann. Stat. 7. 1 (1979).
- 41. R. Senaratne *et al.*, Data for "Spin-charge separation in a 1D Fermi gas with tunable interactions." Zenodo (2022).

### ACKNOWLEDGMENTS

We thank T. L. Yang for his contributions to the apparatus. Funding: This work was supported in part by the Army Research Office Multidisciplinary University Research Initiative (grant no. W911NF-17-1- 0323), the NSF (grant nos. PHY-1707992 and PHY-2011829), and the Welch Foundation (grant no. C-1133). H.P. acknowledges support from the NSF (PHY-1912068) and the Welch Foundation (grant no. C-1669). X.-W.G. is supported by National Natural Science Foundation of China (NSFC) key grant no. 12134015, NSFC grant nos. 11874393 and 12121004, and National Key Research and Development Program of China (NKRDPC) grant no. 2017YFA0304500. D.C.-C. acknowledges financial support from Consejo Nacional de Ciencia y Tecnología (CONACyT) (Mexico, scholarship no. 472271). Author contributions: R.S. and D.C.-C. built the experimental setup performed the measurements, and analyzed data. S.W. and F.H. performed the modeling of the experimental data and the theoretical calculations. Y.-T.C. and A.K. assisted with experiments. All work was supervised by H.P., X.-W.G., and R.G.H. All authors discussed the results and contributed to the manuscript. Competing interests: The authors declare no competing interests. Data and materials availability: All data needed to evaluate the conclusions in the paper are archived on Zenodo (41). License information: Copyright © 2022 the authors, some rights reserved; exclusive licensee American Association for the Advancement of Science. No claim to original US government works. https://www.science.org/about/ science-licenses-journal-article-reuse

### SUPPLEMENTARY MATERIALS

science.org/doi/10.1126/science.abn1719 Materials and Methods Supplementary Text

Figs. S1 to S10 References (42–45)

Submitted 11 November 2021; accepted 16 May 2022 10 1126/science abn1719



## Spin-charge separation in a one-dimensional Fermi gas with tunable interactions

Ruwan SenaratneDanyel Cavazos-CavazosSheng WangFeng HeYa-Ting ChangAashish KafleHan PuXi-Wen GuanRandall G. Hulet

Science, 376 (6599), • DOI: 10.1126/science.abn1719

### Separating spin and charge

In one-dimensional fermionic systems, spin and charge excitations can decouple from each other. This so-called spin-charge separation has been detected in solids and cold-atom systems held in optical lattices. Senaratne *et al.* observed spin-charge separation in one-dimensional Fermi gases of lithium atoms in the absence of a lattice structure within the gas. The researchers were able to excite the spin and charge excitation modes independently from each other and measure their velocities as a function of the strength of the atomic interactions. —JS

### View the article online

https://www.science.org/doi/10.1126/science.abn1719

**Permissions** 

https://www.science.org/help/reprints-and-permissions

Use of this article is subject to the Terms of service